Energetic magnetospheric oxygen in the magnetosheath and its response to IMF orientation: Cluster observations

M. F. Marcucci,[1] M. B. Bavassano Cattaneo,[1] G. Pallocchia,[1] E. Amata,[1] R. Bruno,[1] A. M. Di Lellis,[2] V. Formisano,[1] H. Rème,[3] J. M. Bosqued,[3] I. Dandouras,[3] J.-A. Sauvaud,[3] L. M. Kistler,[4] E. Moebius,[4] B. Klecker,[5] C. W. Carlson,[6] G. K. Parks,[6] M. McCarthy,[7] A. Korth,[8] R. Lundin,[9] and A. Balogh[10]

Received 31 October 2003; revised 13 February 2004; accepted 27 February 2004; published 8 July 2004.

[1] We present Cluster observations made during an outbound orbit on 10 December 2000. After exiting the magnetosphere at midlatitude, Cluster spent a long time skimming the magnetopause moving to lower latitude along an orbit approximately in the ZY_{GSM} plane on the dusk flank of the magnetopause. During this time, magnetospheric oxygen with energy $\geq$10 keV was observed continuously both in the magnetosphere and in the magnetosheath by the Cluster Ion Spectrometry (CIS) plasma experiment. While the oxygen density is roughly constant in the magnetosheath throughout the event, its velocity shows a strong dependence on the magnetosheath magnetic field orientation: low speeds, corresponding to almost isotropic distribution functions, occur for northward magnetic field, and high speeds, corresponding to "beam-like" distribution function occur for southward magnetic field. Mainly, two different processes have been discussed to explain the energetic particles escaping from the magnetosphere: flow along reconnected magnetospheric and magnetosheath field lines or crossing of the magnetopause when the particle gyroradii are comparable with the magnetopause thickness. The presence of the oxygen population cannot be readily explained in the framework of the reconnection theory. Instead, the observations are successfully reproduced by a model based on magnetopause crossing by finite gyroradius, provided the magnetosheath convection is taken into account together with the magnetosheath magnetic field orientation. Moreover, the presence of quasi-periodic motion of the magnetopause surface with period of approximately 5 min are evidenced by the analysis. *INDEX TERMS:* 2724 Magnetospheric Physics: Magnetopause, cusp, and boundary layers; 2116 Interplanetary Physics: Energetic particles, planetary; 2784 Magnetospheric Physics: Solar wind/magnetosphere interactions; 2728 Magnetospheric Physics: Magnetosheath; *KEYWORDS:* magnetopause crossing by magnetospheric oxygen, remote sensing of magnetopause motion

Citation: Marcucci, M. F., et al. (2004), Energetic magnetospheric oxygen in the magnetosheath and its response to IMF orientation: Cluster observations, *J. Geophys. Res.*, *109*, A07203, doi:10.1029/2003JA010312.

1. Introduction

[2] Magnetospheric energetic particles have often been observed in the magnetosheath near the magnetopause. They can escape from the magnetosphere along reconnected magnetic field lines [*Speiser et al.*, 1981; *Scholer*, 1983; *Daly et al.*, 1984] or leak in the magnetosheath, namely crossing the magnetopause by means of their large gyroradius and being lost from the magnetosphere [*Eastman and Frank*, 1982; *Papamastorakis et al.*, 1984]. *Sibeck et al.* [1987], through the reexamination of observations made in the past together with the study of new observations made by the CCE satellite during the AMPTE program, evidenced that the leakage model predictions account for the observations as well as the predictions by the merging model. They also showed that at the low-latitude subsolar region, the motion of the ions crossing the magnetopause should depend on the orientation of the magnetosheath field: they

[1]Istituto di Fisica dello Spazio Interplanetario, Consiglio Nazionale delle Ricerche, Roma, Italy.
[2]AMDL s.r.l., Roma, Italy.
[3]CESR, Toulouse, France.
[4]University of New Hampshire, Durham, New Hampshire, USA.
[5]Max-Planck-Institüt für Extraterrestrische Physik, Garching, Germany.
[6]University of California, Berkeley, California, USA.
[7]University of Washington, Seattle, Washington, USA.
[8]Max-Planck-Institüt für Aeronomie, Katlenburg-Lindau, Germany.
[9]Swedish Institute of Space Physics, Kiruna, Sweden.
[10]Imperial College, London, UK.

0148-0227/04/2003JA010312$09.00

should move dawnward and northward in a duskward field and dawnward and southward in a dawnward field. More recently, *Paschalidis et al.* [1994], studying several crossings both of the dawnside and duskside equatorial magnetopause, showed that $\geq$50 keV ions, observed by the CCE/AMPTE satellite, are of magnetospheric origin and that a continuous leakage across a tangential discontinuity magnetopause is the most probable escaping mechanism. *Zong et al.* [2001] instead reported on Geotail observations of energetic magnetospheric oxygen ions outside the dayside magnetopause and interpreted such observations in terms of large-scale steady reconnection at the subsolar magnetopause opening a path for the escape of the ring currents ions into the magnetosheath.

[3] Here we present Cluster observations in which magnetospheric oxygen with energy $\geq$10 keV was observed in the dusk flank, mid latitude magnetosheath. The oxygen particles were present in the magnetosheath for over three hours and their distribution functions changed depending on the magnetosheath magnetic field orientation. We discuss on the cause of the oxygen escape and present a simple model which reproduces the observations throughout the event on the basis of large gyroradius crossing of the magnetopause. Moreover, the analysis reveals the occurrence of quasi-periodic motion of the magnetopause surface during the period of observations.

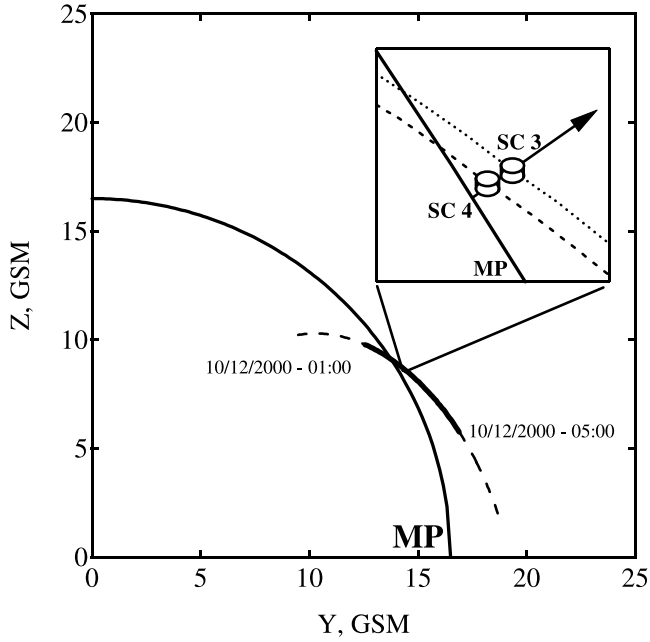

Figure 1. Cluster orbit in the ZY GSM plane for the period under study (heavy solid line). A model magnetopause (solid line) is also reported. In the insert, SC 3 and SC 4 positions relative to the model magnetopause are shown together with the Fairfield magnetopause normal.

2. Observations

[4] The data we present were taken by the Cluster Ion Spectrometry (CIS) plasma instrument [*Rème et al.*, 2001] and by the Fluxgate Magnetometer (FGM) experiment [*Balogh et al.*, 2001] on board Cluster during 10 December 2000. CIS experiment consists of two different instruments: a Composition and Distribution Function Analyzer (CODIF) which gives the three-dimensional distribution functions for H^+, He^{++}, He^+, and O^+ in the energy per charge range 20–40,000 eV/e and a Hot Ion Analyzer (HIA) which gives the ion three-dimensional distribution functions in the energy per charge range 5–32,000 eV/e with no mass separation. The data of the present study were taken in the early part of the Cluster mission, during the commissioning phase, and CIS was operating only on SC 3 and SC 4. Observations were made while Cluster was moving along an outbound orbit on the duskside of the magnetosphere very close to the YZ_{GSM} plane. We will concentrate in the time interval 0100–0500 UT: during this period, high-energy magnetospheric oxygen ions were observed in the magnetosheath by CODIF. In Figure 1 the Cluster orbit is projected onto the YZ_{GSM} plane (dashed line); the solid line segment of the orbit identifies the period under study, during which Cluster moved from $\sim$36° to $\sim$19° GSM latitude always skimming the magnetopause, whose model is also drawn. The insert in Figure 1 shows the positions of SC 3 and SC 4 (spacecraft separation $\sim$350 km) relative to the model magnetopause and will be described in more detail in section 5, where the comparison of SC 3 and SC 4 observations will be discussed. We concentrate on SC 3 data, which are reported in Figure 2, since SC 3 and SC 4 observations are similar. From top to bottom, ion temperature, density and bulk velocity, oxygen density and velocity in the energy range 10–40 keV and, in the bottom panel, the magnetic field clock angle (defined as $\tan^{-1}$ (B_y/B_z)) are plotted. The ion data were provided by HIA with a 4 s time resolution; CODIF was providing the O^+ data with a time resolution of 16 s; the magnetic field data are 4 s averages. Looking at the ion data, it can be seen that Cluster remains in the magnetosheath, where high velocity and density and low temperature values are observed, after the magnetopause crossing of 0130 UT, apart from some brief excursions in the magnetosphere/magnetosphere boundary layer (MSP/BL) (lower density and velocity, higher temperature values). Inside the magnetopause the magnetic field is directed almost northward and its magnitude (not shown) is approximately equal to that of the magnetosheath magnetic field. As far as the O^+ observations are concerned, the detailed inspection, throughout the event, of the three-dimensional distribution functions and of the Time of Flight (TOF) histograms (not shown) reveals that the magnetosheath O^+ population of the present study does not extend to energies below $\sim$10 keV. On the other hand, spurious counts are observed by the CODIF O^+ TOF channel at energies corresponding to magnetosheath H^+, in this event below $\sim$10 keV. Such spurious counts due to the contamination from high H^+ fluxes should be excluded from the analysis [e.g., see *Rème et al.*, 2001]. Therefore all the oxygen moments referred to hereafter are computed in the 10–40 keV energy range. The O^+ density and velocity reveals some interesting features. First of all, the O^+ particles, whose source is inside the magnetosphere, are observed throughout the period under study. The O^+ density is always above $\simeq 10^{-3}$ cm^{-3} apart from some short intervals (e.g., 0418 $\div$ 0426 UT) and remains roughly constant throughout the interval: therefore the magnetospheric oxygen is continuously escaping in the magneto-

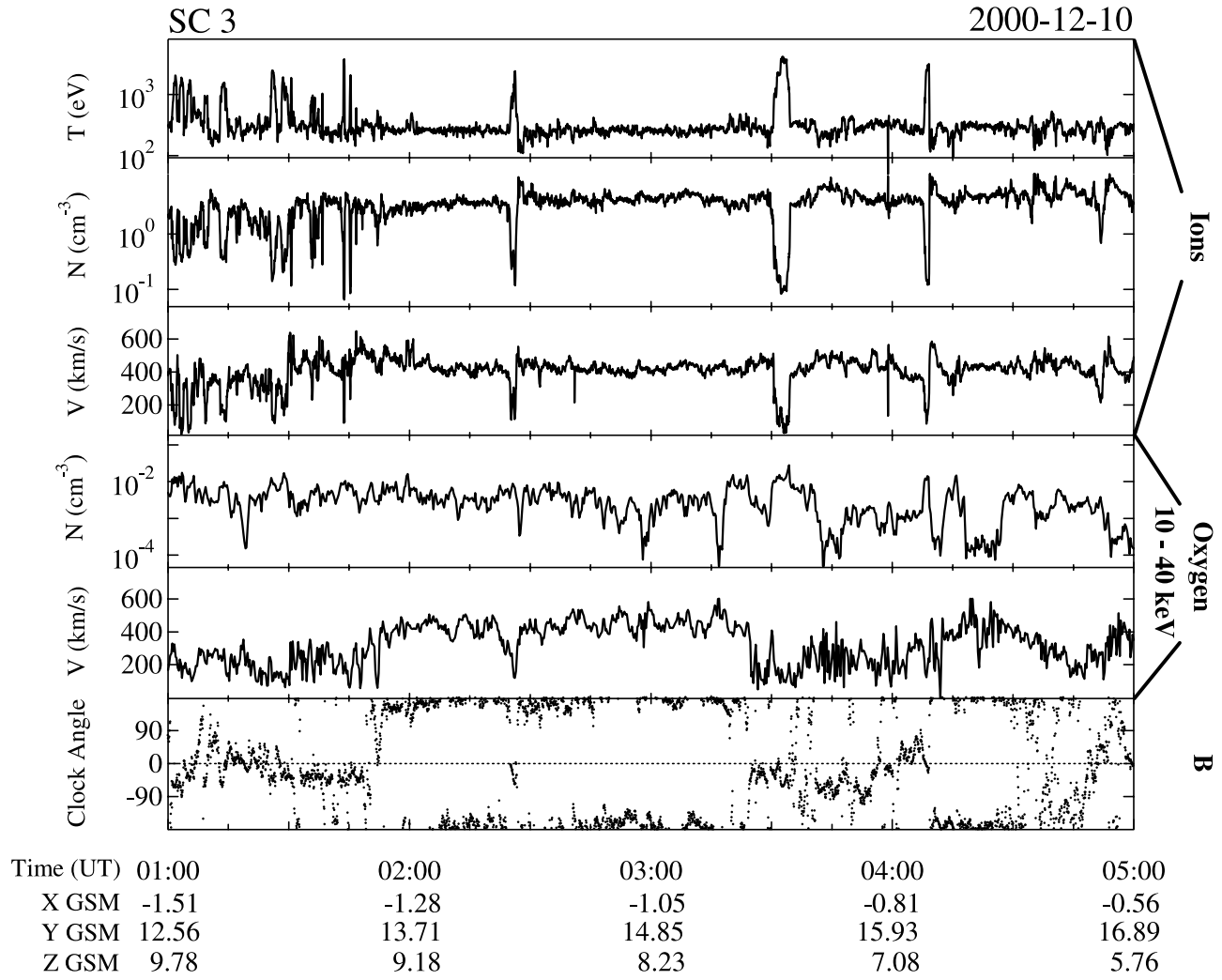

Figure 2. From top to bottom: the ion temperature, density, and bulk velocity; the oxygen density and velocity computed for the energy range 10–40 keV; the magnetic field clock angle (dotted line) measured on board SC 3.

sheath through some process active at the magnetopause. At the same time the velocity of O^+ is characterized by large variations, attaining values ranging from ~600 km/s to ~100 km/s, the density having roughly the same values, as already mentioned. Comparing the O^+ velocity and the magnetic field clock angle, it is important to note that the high speed values are observed whenever the magnetosheath magnetic field is directed southward. In fact, the analysis of the particles distribution functions throughout the period under study shows that in the MSP/BL the oxygen distribution functions are almost isotropic, with bulk velocity $\leq$50 km/s, and covering the velocity range from ~200 km/s to the upper limit of the instrument (~700 km/s), and possibly beyond this limit; in the magnetosheath during southward magnetic field the distribution function is restricted only to a small angular sector and often to very high velocity values, appearing as a "beam-like" distribution function; in the magnetosheath during northward magnetic field, instead, the distribution function does not show any preferred direction with values scattered both in energy and angle. In the next section the possible cause for the O^+ crossing of the magnetopause and for the magnetic field orientation dependence will be discussed.

3. Escaping Process

[5] To investigate on the nature of the escaping mechanism, we analyze the oxygen observations in more detail. In Figure 3 only O^+ data are displayed. In the upper panel the O^+ velocity (solid line) and the computed $-\mathbf{V} \times \mathbf{B} \times \mathbf{B}$ (V_{drift}) velocity (grey shaded) are plotted. In the two middle panels the O^+ velocities perpendicular and parallel to the magnetic field are displayed. The lower panel displays again the magnetic field clock angle. Looking at the upper panel, it can be noted that remarkably the O^+ velocity sometimes is smaller than the V_{drift} velocity. This occurs during northward magnetic field. During southward periods the O^+ velocity is greater than V_{drift} velocity except for the short period ~0152 ÷ 0157. As far as the perpendicular velocity is concerned, a clear relation with the orientation of the magnetosheath magnetic field can be observed: when it is southward directed, V_{perp} is well above 400 km/s, otherwise

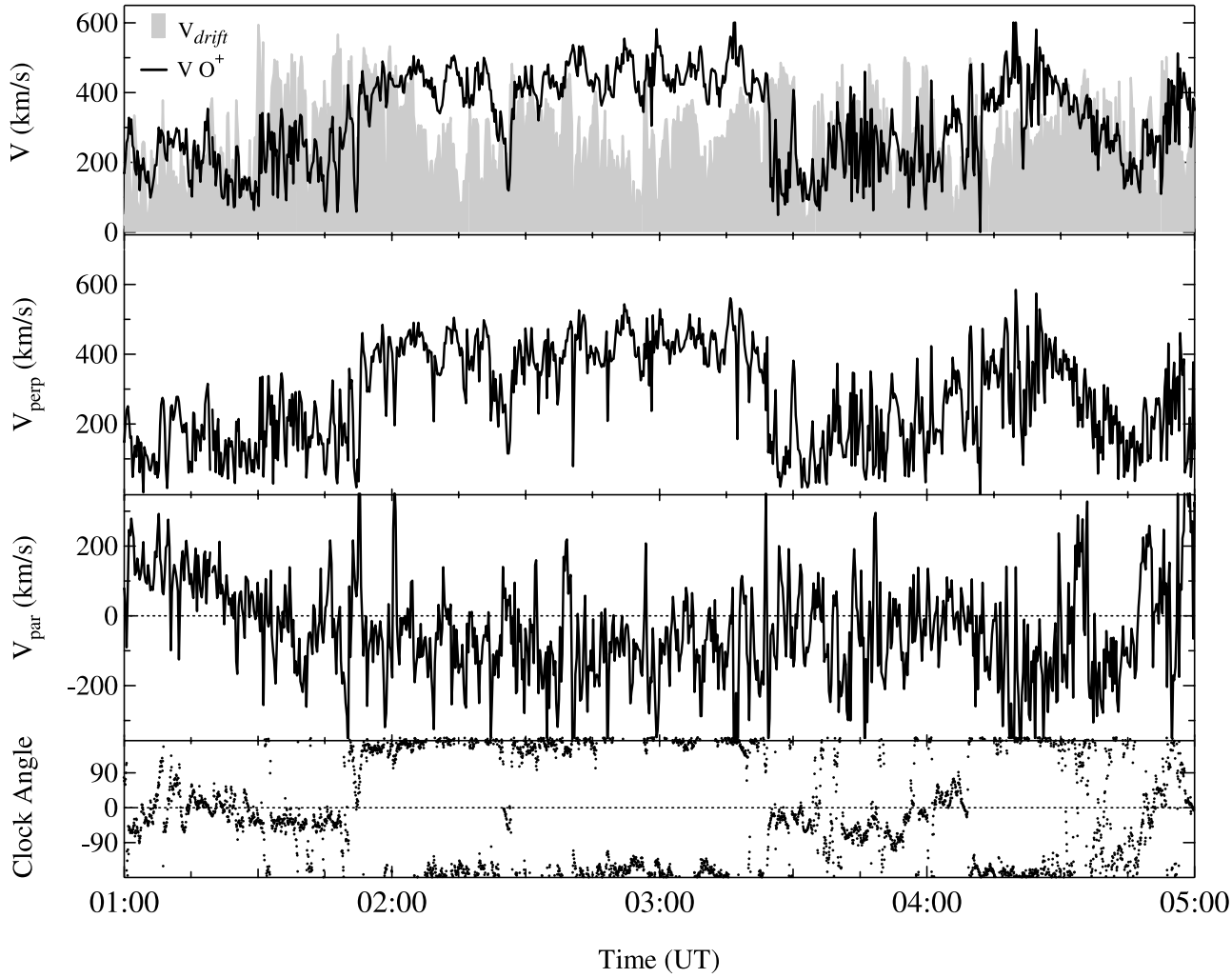

Figure 3. The O^+ velocity (solid line) and the computed V_{drift} velocity (grey shaded) are reported in the upper panel. In the two middle panels, the SC 3 O^+ velocities perpendicular and parallel to the direction of the magnetic field are displayed. Lower panel: magnetic field clock angle as in Figure 2.

it is below 200 km/s; on the other hand, the parallel velocity does not show any relation with the magnetic field orientation being most of the time much smaller than the perpendicular velocity and highly variable. Some tentative conclusions may be already drawn starting from these observations.

3.1. Escaping Via Reconnection

[6] Magnetospheric oxygen may flow in the magnetosheath along reconnected magnetic field lines. There is overwhelming evidence that the reconnection process occurs at the terrestrial magnetopause. In situ evidence for reconnection is based on the observation in the magnetopause current sheet of magnetosheath plasma flows which are driven by the tension of the bent reconnected magnetospheric and magnetosheath field lines [e.g., *Paschmann et al.*, 1979; *Sonnerup et al.*, 1981; *Paschmann et al.*, 1982, 1986; *Gosling et al.*, 1982, 1990]. Such flows sometimes are accelerated with respect to the adjacent magnetosheath and sometimes are deflected and/or decelerated, depending on the magnetosphere and magnetosheath magnetic field topology. In fact, when the terrestrial and the interplanetary magnetic fields are connected, the magnetopause can be described as a rotational discontinuity and, in the framework of MHD, the tangential components of the transmitted plasma flows are determined by the variations of the tangential magnetic field components across the magnetopause according to the Walén relation [*Hudson*, 1970]. In the present case the test of the Walén relation across the magnetopause crossings (not shown) does not provide any evidence of reconnection signatures. It must be noted, however, being the Walén test local in nature, that reconnection can be occurring at some other location or has occurred in the past. It could also be the case that the magnetopause crossings during this event are too fast to permit the detection of the reconnection flows. Besides, it has to be noted that at some magnetopause crossings a very low density BL is detected, but this fact alone can not be taken as an indication of open magnetic field lines [*Lockwood et al.*, 2001, and references therein].

[7] As far as the large-scale configuration of the reconnection at the magnetopause is concerned, the location where the magnetospheric and magnetosheath field lines become interconnected should depend on the relative ori-

entation of the two magnetic fields according to the two models: the ''antiparallel merging'' [*Crooker*, 1979; *Luhmann et al.*, 1984] and the ''component merging'' [*Gonzales and Mozer*, 1974; *Sonnerup*, 1974]. In the event under study the orientation of the magnetosheath magnetic field undergoes several variations which should imply different reconnection sites even far away from the spacecraft position; despite this the density of the O^+ observed in the magnetosheath does not change as it could be expected. Moreover, it has been shown that the O^+ ions velocity is either very low or is high but directed almost perpendicular to the magnetic field; parallel velocities are small in comparison with the total velocity and highly variable. This seems to be inconsistent with a unidirectional streaming along reconnected field lines as expected for reconnection. Because of all these facts it is difficult to readily interpret the escaping process in terms of reconnection.

3.2. O^+ Crossing of the Magnetopause: A Model

[8] The other mechanism proposed to account for the presence of energetic magnetospheric particles in the magnetosheath is crossing due to the finite gyroradius effect: energetic particles whose gyroradii are comparable with the magnetopause thickness simply cross it, get out of the magnetosphere and gyrate around the magnetosheath field and possibly reenter the magnetosphere. If this is indeed the case, the magnetic field orientation dependence must be explained. Similarly to *Sibeck et al.* [1987], we elaborate on the energetic ions motion in the magnetosheath and propose a simple model which could account for the observations. The model predictions are presented in Figure 4 for the two cases of northward and southward magnetosheath magnetic field. Hereinafter, the GSE reference system will be used. Let a planar magnetopause along the XZ plane separate the magnetosphere from the magnetosheath and let the intensity of the magnetic field be approximately the same on the two sides of the current sheet. In the magnetosphere the magnetic field is directed northward. In Figure 4a the orbit of a particle whose gyrocenter is just outside the magnetopause is shown in the XY plane: for northward directed magnetosheath field (left side) the particle, once it goes out of the magnetosphere, will gyrate around the magnetosheath field having $V_x \geq 0$. In the case of southward external field (right), the particle gyration will be opposite and it will have $V_x \leq 0$ in the magnetosheath. The difference in the single particle orbits will result in different distribution functions when a collection of particles of different energies is considered. In Figure 4b the cut of the distribution functions on the V_xV_y plane, as they would be observed by a satellite just outside the magnetopause, is sketched for the two different magnetic field orientations; the distribution function inside the magnetosphere is also sketched and can be considered as a proxy of the distribution functions observed in the magnetosphere for the interval under study. In the northward (left) case only particles with $V_x \geq 0$ are present just outside the magnetopause while V_y, the velocity component along the magnetopause normal, can be either positive or negative, since particles go out and reenter the magnetopause gyrating around the magnetic field; therefore only the $V_x \geq 0$ part of the original magnetospheric distribution is observed in the magnetosheath. In the southward case (right), just outside the magnetopause particles will have only $V_x \leq 0$: also in this case half of the magnetospheric distribution is observed, but now it has only $V_x \leq 0$. To summarize, only half of the distribution function is transmitted across the magnetopause, with $V_x \geq 0$ or $V_x \leq 0$ depending on the magnetosheath magnetic field orientation. The same shape of the distribution function is predicted also for the V_xV_z plane: once again the sign of V_x depends on the orientation of the magnetic field, while V_z can be either positive or negative because particles maintain their parallel velocity on entering the magnetosheath. Eventually, in the V_yV_z plane the isotropy of the distribution function is maintained since particles can move in any direction along the magnetic field and the magnetopause normal. In a three-dimensional view, a $V_x \geq 0$ half-sphere is transmitted in the northward case and a $V_x \leq 0$ half-sphere is transmitted in the southward case. In order to compare the model with the observations, it is necessary to take into account the effects of magnetosheath convection. In fact, during the period of observation, V_{drift} attains values sometimes as high as 500 km/s. In our simplified case, let V_{drift} be directed along negative X. In Figure 4c the predicted distribution functions are shown taking into account the convection. In the northward case (left) the distribution function will be shifted toward $V_x \leq 0$ and becomes more isotropic; O^+ going along X with the highest velocity could still be observed (dotted area) if particles with energy beyond the upper limit of the instrument are present in the

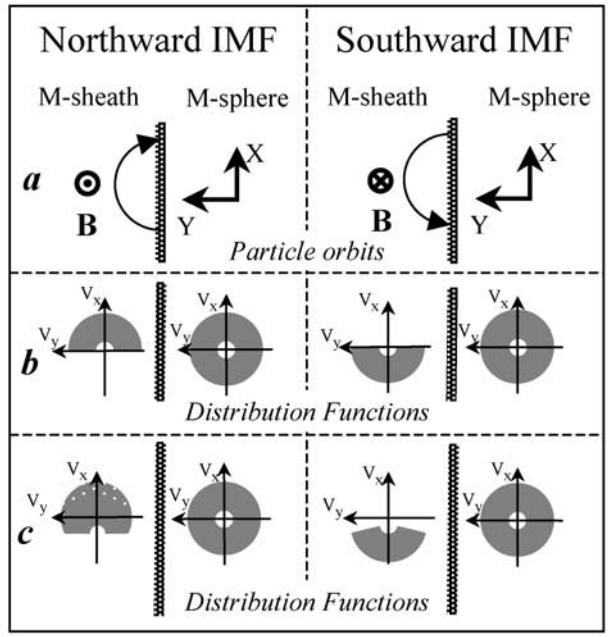

Figure 4. Sketch of particle orbits and distribution functions for northward (left side) and southward (right side) magnetosheath magnetic field. (a) The single particle orbits in the XY GSE plane are shown. (b) The expected cuts of the distribution functions in the V_xV_y plane are represented for the two cases together with a sketch of the distribution function observed inside the magnetopause. (c) The distribution functions are shown after the effect of the magnetosheath convection in the antisunward direction has been taken into account.

magnetosphere. In the southward case (right) the distribution function, already in the $V_x \leq 0$ plane, is further shifted toward negative V_x values: the lower energy limit of the observed velocities will increase, while the part of the distribution function exceeding the upper energy limit of the instrument will be lost: this results in a more ''beam-like'' distribution function. Therefore this simplified model is in qualitative agreement with the observations predicting more isotropic oxygen distribution during northward magnetosheath magnetic field and more ''beam-like'' distribution function during southward magnetosheath magnetic field. In the following, we will first show a comparison between the observed and predicted distribution functions for different orientations of the magnetic field and then the comparison between the observed oxygen velocity and the velocity computed from a model distribution function throughout the event.

4. Comparison Between the Model and the Observations

[9] In the general case, just outside the magnetopause, when the magnetosheath convection can be neglected and the intensity of the magnetic field is approximately the same on the two sides of the magnetopause, the shape of the model distribution function is determined by the directions of the magnetopause normal, **n**, and of the magnetosheath magnetic field, **B**. Particles can attain both positive and negative velocity along the magnetopause normal, as already mentioned. The particle velocity along **B** can attain any positive or negative value when **B** and the magnetospheric field are aligned (see section 3.2). When **B** is perpendicular to the magnetospheric field, namely in the *XY* plane, the majority of particles is expected to flow parallel (antiparallel) to **B** when it has positive (negative) *X* component, since the majority of particles cross the magnetopause with positive *X* velocities, while only a small fraction goes in the opposite direction due to particle scattering [*Sibeck et al.*, 1987]. We will make the simplifying assumption that particles can freely move back and forth along **B**, so that in the **nB** plane the model distribution function will be isotropic. This assumption will be shown to be acceptable when comparing the model predictions with the observations. Moreover, outside the magnetopause the particles gyration is such that only particles whose velocity component along the magnetopause is directed as $\mathbf{n} \times \mathbf{b}$ ($\mathbf{b} = \mathbf{B}/B$) will be observed. Therefore the model distribution function is represented by a half-sphere cut along the **nB** plane located on the side of the $\mathbf{n} \times \mathbf{B}$ vector. Finally, to take into account the magnetosheath convection, the model distribution function must be shifted in the appropriate direction like in the simplified case of section 3.2.

[10] In Figure 5, observations and model predictions are compared. We remind that SC 3 is always very close to the magnetopause throughtout the event. The normal to the Fairfield magnetopause model [*Fairfield*, 1971] for this event is **n** = (0.45, 0.77, 0.44) at 0230 UT and does not change significantly throughout the event; the magnetosheath convection is directed principally along negative *X* and positive *Y*. The magnetosheath magnetic field rotates during the event and in Figure 5 four times are reported when it is predominantly northward, southward, tailward, and sunward. For each time a sketch of the three-dimensional distribution function of escaping oxygen ions is shown together with the observed distribution function in the energy range 10–40 keV. In each case the drift velocity and magnetic field averages over the time interval of the distribution function measurement are reported. The observed distribution functions are displayed in the φ-θ plane in order to simplify the comparison with the model. The φ and θ angles are the longitude and latitude in the GSE frame, respectively. Let us now examine the different cases. In the two upper cases, V_{drift} is large and directed tailward and duskward: this is due to the large B_z component, regardless of its sign. In the northward case the escaping particle distribution function is almost contained in the V_x positive space; the $-\mathbf{V} \times \mathbf{B} \times \mathbf{B}$ drift will shift it toward negative V_x so that the resulting distribution function will become more isotropic. In the southward case, the distribution function is almost contained in the V_x negative space and the drift moves it further towards negative V_x: the resulting distribution function will be concentrated around the V_{drift} direction. Comparison with the observations shows that this is exactly the case: during northward magnetic field the distribution function spreads over almost all the observation directions and even sunward moving particles are observed; in the southward case the distribution function is concentrated in $\varphi \sim 140$ and $\theta \sim -20$ which means that the velocity is directed mostly along V_x negative, with V_y positive and V_z slightly negative. In the two bottom cases the magnetic field has a predominant B_x component, therefore the $-\mathbf{V} \times \mathbf{B} \times \mathbf{B}$ drift is drastically reduced: particles that cross the magnetopause will simply gyrate around the magnetic field and will only have $V_z \geq 0$ when the magnetic field is directed tailward and $V_z \leq 0$ when the magnetic field is directed sunward. Once again this is in agreement with the observations: during tailward magnetic field the distribution function is mostly contained in the $\theta \geq 0$ sector while for sunward magnetic field it is restricted to $\theta \leq 0$ values. We note that in all the cases, there is no clear asymmetry with respect to the field direction thus justifying the simplified assumption of isotropy of the distribution function in the **nB** plane.

[11] To check the validity of the model throughout the event we simulated the expected distribution function and computed the corresponding ions velocity to compare it with the observations. Starting from the hypothesis that the s/c is at a fixed distance from the magnetopause and within 1 gyroradius of the lowest energy limit of the instrument, for each time of observations we simulated the expected particle distribution in three steps. First an isotropic particle distribution is created over $16 \times 8 \times 8$ measurement bins with eight different velocity values in the range 100–800 km/s and 16×8 different directions identified by 16 azimuthal angles in the range 0°–360° and eight polar angles in the range −90°–90°. This is a proxy of the magnetospheric ions distribution function. Second, the vector $\mathbf{n} \times \mathbf{b}$ is computed, using the magnetic field averaged over the acquisition time of each O^+ distribution function and the normal to the Fairfield magnetopause model for 0230 UT; the angle between this vector and each ion velocity is calculated and only particles for which this angle is $\leq 90°$ are retained for the subsequent analysis. This distribution accounts for the density gradient and magnetic

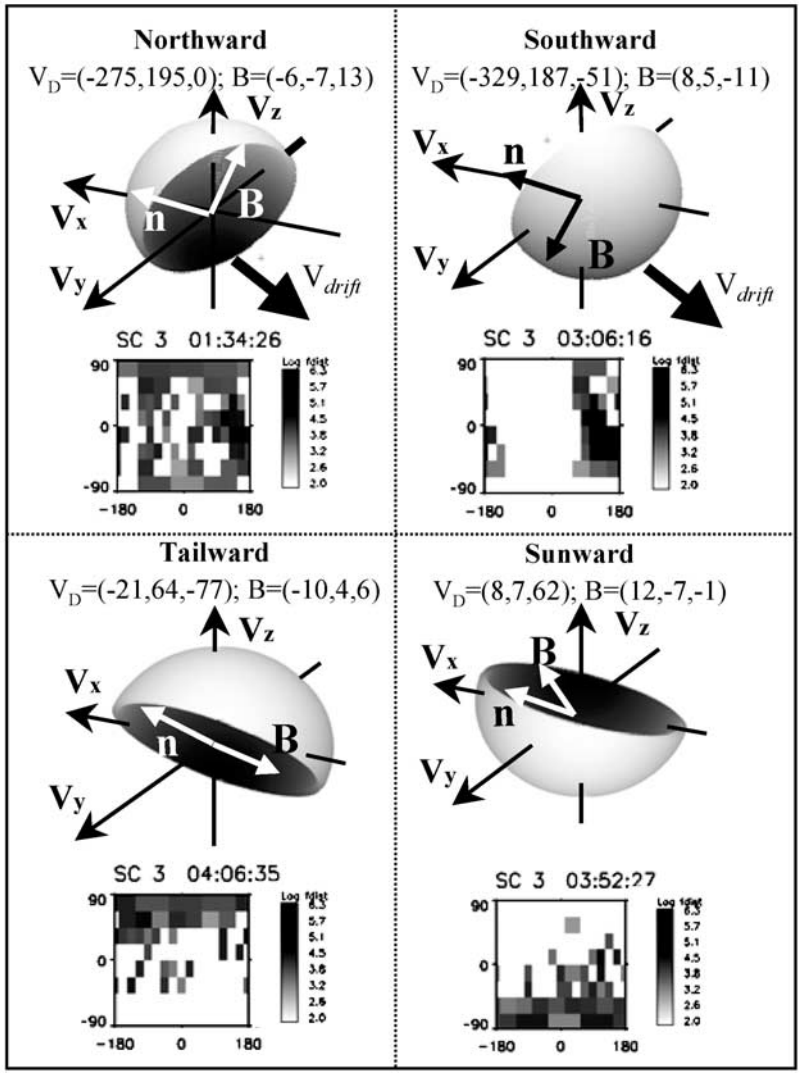

Figure 5. The sketch of the predicted distribution functions together with the SC 3 observations are reported for different orientation of the magnetosheath magnetic field. In each panel are shown: the V_{drift} velocity, V_D, and magnetic field averaged over the time interval of the distribution function measurement, the sketch of the predicted three-dimensional distribution function and the observed distribution function for the energy channel 10–40 keV plotted as a function of longitude and latitude in the GSE frame.

field orientation effects. The third step is to add the $-\mathbf{V} \times \mathbf{B} \times \mathbf{B}$ drift to each particle velocity. The velocity of the simulated distribution function is computed in the energy range 10–40 keV and compared with the observations. Figure 6 displays the proton temperature (Figure 6a) and the oxygen density (Figure 6b), the observed oxygen velocity and its components (continuous line), the $-\mathbf{V} \times \mathbf{B} \times \mathbf{B}$ velocity and its components (shaded area), the simulated oxygen velocity and its components (line marked with open dots) in Figures 6c–6f, respectively; the magnetic field components (Figures 6g–6i). Periods when the oxygen density is very low must be excluded from the comparison since the measured velocity could be unreliable. Such periods and periods when the s/c is inside the magnetopause have not been reported in Figures 6c–6f. It is evident that the overall trend of the oxygen velocity, both its absolute value and its components, is very well predicted by the model, apart from some enhancement of the oxygen velocity during the southward magnetic field period of 0150–0323 UT which will be discussed in section 4.1. In particular, the model predicts the very low oxygen velocity during northward magnetic field intervals, e.g., 0130–0150 UT and 0323–0328 UT; notably, during these time intervals the oxygen velocity is even lower than the V_{drift} velocity. The model is very successful in predicting the oxygen velocity also during periods when the magnetic field is mainly contained in the XY plane; such periods are present in the interval 0348–0407 UT, when the magnetic field, while being tangent to the magnetopause surface, is first directed toward the sun and then rotates northward and eventually tailward. During this period the oxygen velocity is almost along the Y and Z plane and changes according to the magnetic field orientation as it is expected by the model; also in this case the $-\mathbf{V} \times \mathbf{B} \times \mathbf{B}$ drift alone cannot account for the observations being almost oppositely directed to the observed velocity during all the interval. The differences

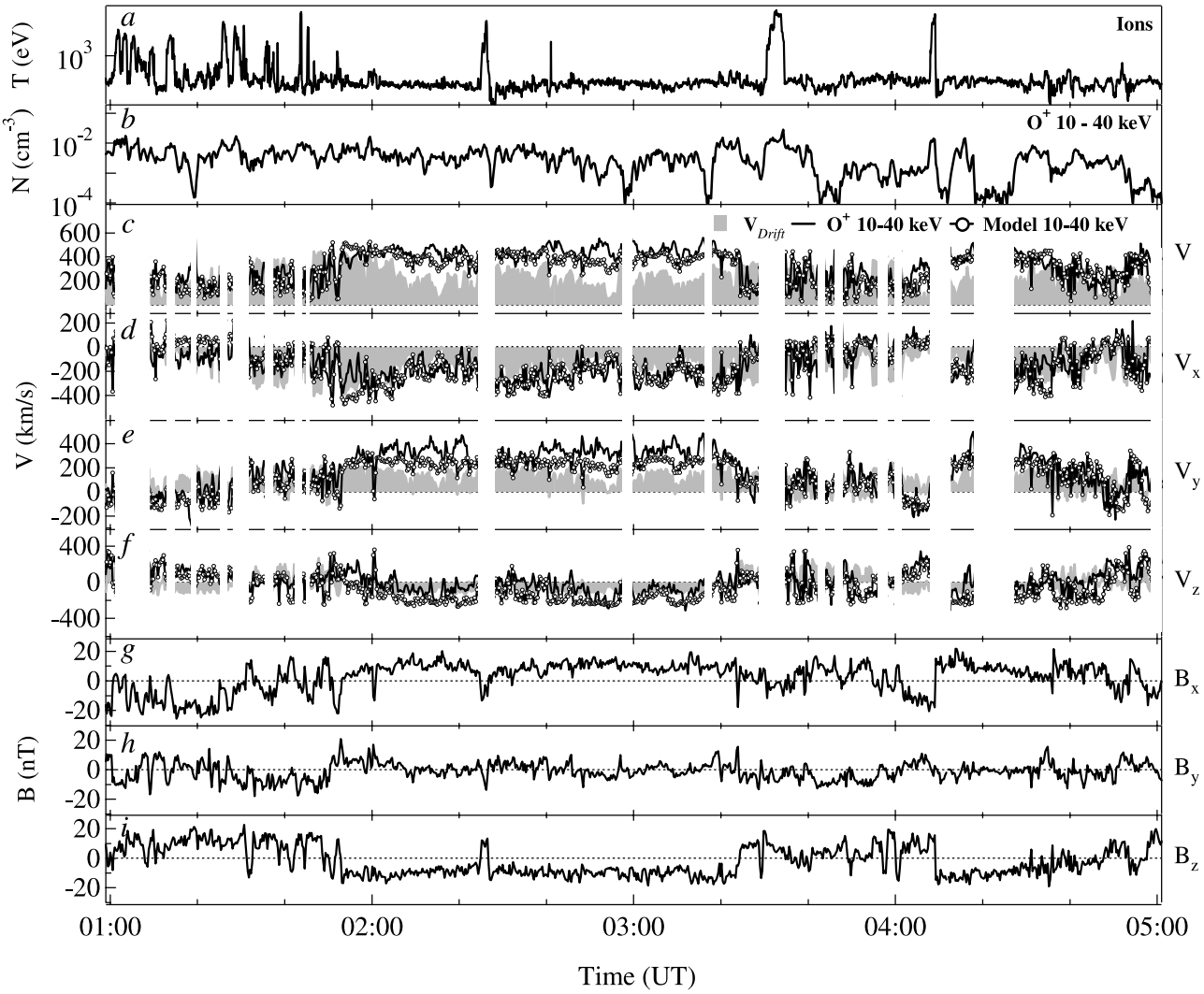

Figure 6. Comparison between the reconstructed and the observed SC 3 O^+ velocity. (a) Proton temperature; (b) oxygen density; (c)–(f) the observed oxygen velocity and its components (continuous line), the $-\mathbf{V} \times \mathbf{B} \times \mathbf{B}$ drift velocity and its components (shaded area), the simulated oxygen velocity and its components (marked line); (g)–(i) the magnetic field components.

between the model and the observations which arise sometimes, during very short periods, could be due to the fact that a constant magnetopause normal has been used in the model, whereas the actual magnetopause normal is likely to change on a small temporal scale, due to magnetopause motions, such as the ones which cause the brief excursions of the s/c into the magnetosphere. Therefore we conclude that the model is able to predict well the overall trend of each component of the observed oxygen velocity implying that the oxygen particles cross the magnetopause because of their large gyroradius. The next section will be dedicated to the study of the oxygen velocity enhancements not predicted by the model and to the description of a possible interpretation.

4.1. Remote Sensing of Magnetopause Motion?

[12] In Figure 7 a blow up of the oxygen velocity and density measured by SC 3 is plotted for the time period 0140–0330 UT. Similarly to Figure 6, periods when the oxygen density is very low and when the s/c is inside the magnetopause have not been plotted. It is evident that several velocity peaks, in which the oxygen velocity increases from a minimum (∼400 km/s) to the peak value (∼500 km/s) and then decreases, are superposed on the southward B high velocity interval. In the figure these velocity peaks are highlighted by shaded areas. The duration of the velocity enhancements, the interval between the two velocity minima in the shaded areas, is almost the same for all the peaks and is approximately 5 min. A detailed analysis of the distribution functions may help to understand the cause of such periodic variations. In Figure 8 the observed distribution function cuts in the V_xV_y plane have been plotted for the interval 0249:28–0254:33 UT which corresponds to the fourth shaded region in Figure 7. The squared distribution function corresponds to the velocity maximum. It can be noted that the velocity increase corresponds to progressive reductions both in the energy range, namely lower energy particles disappear, and in the angular width of the measured distribution functions. This could be explained

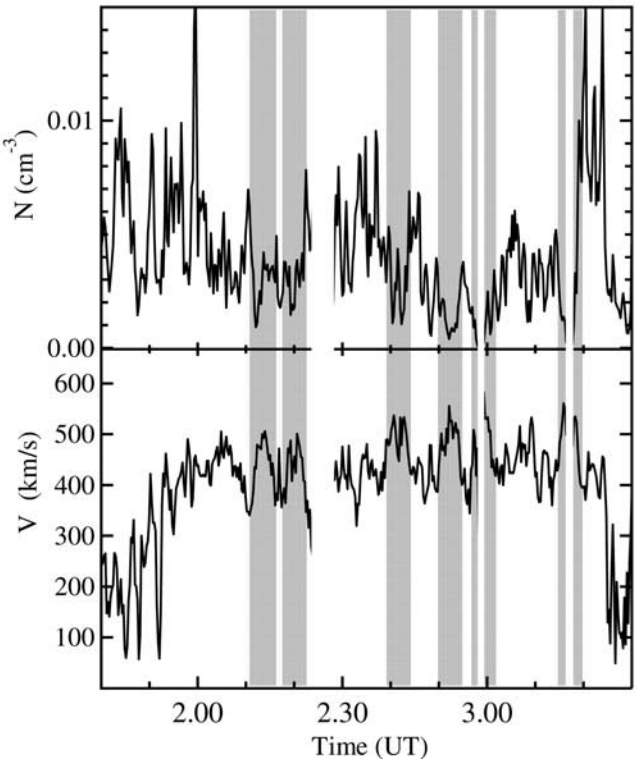

Figure 7. Oxygen density (upper panel) and velocity (lower panel) measured by SC 3 in the energy range 10–40 keV during the prolonged period of southward magnetosheath magnetic field.

as a distance effect: as the distance from the magnetopause increases lower energy particles, which have smaller gyroradii, are progressively lost by the instrument until only particles with the largest energies (i.e., largest gyroradii) and directions tangent to the magnetopause will be observed by the spacecraft; in fact, the velocity peaks correspond to lower density values. Such interpretation is also supported by the disappearance of O^+ particles occurring at two of the velocity maxima (0258 and 0316 UT): at these times the distance from the magnetopause has increased until no more O^+ particles are detected within the energy range of the instrument. The progressive disappearance of lower energies, which causes the apparent acceleration, has not been considered in the model, which assumes that the observations are made at a fixed distance from the magnetopause (see section 4) and that particles of all energies are observed. This is the reason of the disagreement between model predictions and observations. We interpret the apparent ions acceleration as due to oscillations of the magnetopause which vary the distance between the spacecraft and the magnetopause and hence the characteristics of the oxygen distribution function.

5. Comparison Between SC 3 and SC 4

[13] The position of SC 3 and SC 4 relative to a model magnetopause is presented in the insert in Figure 1 for 0215 UT. While moving to lower latitudes, skimming the magnetopause, the two spacecraft have their largest separation (~350 km) mainly along the Fairfield magnetopause normal: therefore the spacecrafts' spatial configura-

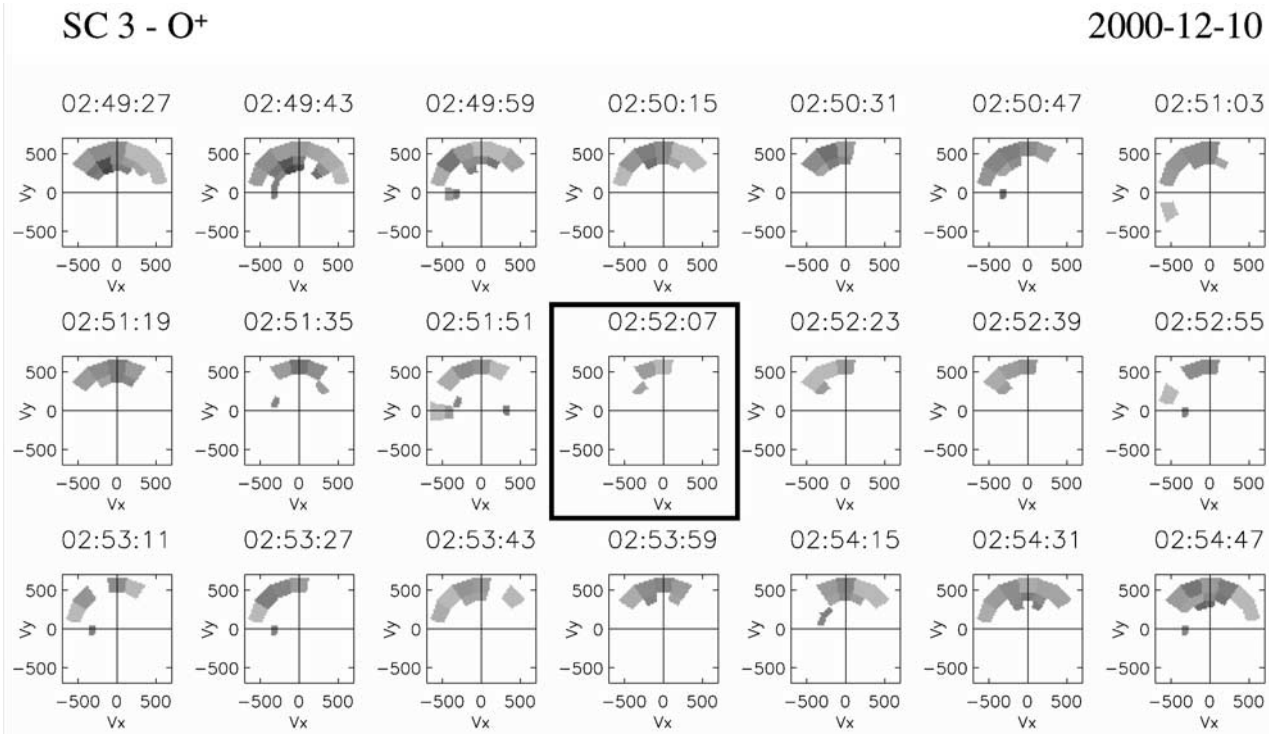

Figure 8. SC 3 O^+ cuts of the distribution function in the V_xV_y plane for the time interval 0249:28–0254:33 UT corresponding to the fourth shaded region in Figure 7. The squared distribution function corresponds to the velocity maximum of 0252:08 UT. The H^+ contamination at low energies has been removed.

tion would be most favorable for the observation of differences due to different distances from the magnetopause. For example, in the framework of our model, it could be expected that lower-energy ions are only observed by the satellite which is closer to the magnetopause. Actually, this is not the case: the comparison of the observations of the two satellites, not shown, does not reveal any appreciable difference: the observations in the various energy channels are the same for the two spacecraft. Nevertheless, some simple considerations lead to the conclusion that this is not in contrast with our interpretation. When considering oxygen ions the relation between the Larmor radius and the energy of the particle, E, is $R_L = 576\sqrt{E}/B$ (where R_L is in km, E is in eV, and B is in nT). Therefore the analysis of the particle energy spectra should enable us to compute the distance between each spacecraft and the magnetopause. In the case when the magnetosheath convection is low, for example, the Larmor radius corresponding to the lowest observed energy gives the distance from the magnetopause of each spacecraft. However, it must be taken into account the intrinsic instrument precision in the determination of the particle energy ΔE which leads to a range of values (ΔD) for the Larmor radius relative to a particular energy channel. In detail $\Delta D = (288\sqrt{E}(\Delta E/E))/B$ where $\Delta E/E$ is a characteristic constant depending on the telemetry product. In our case the lowest energy channel observed is at 10 keV; with a mean field $B \simeq 15$ nT, this gives a $\Delta D \simeq 860$ km, which is larger than the spacecraft separation computed along the normal to the Fairfield magnetopause model ($\sim$350 km). Therefore the two spacecraft are too close to detect any difference and will detect particles in the same energy channels most of the times. Moreover, it must be taken into account that the instrument needs a finite time interval to measure the full distribution function so that possible differences are smeared out. Therefore no appreciable difference between the energy spectra of the two spacecraft is expected, in agreement with the observations.

6. Discussion and Conclusions

[14] In this paper we presented observations made by two Cluster spacecraft on the dusk flank of the magnetopause. While Cluster was moving along the dawn-dusk meridian, always skimming the magnetopause, high-energy magnetospheric oxygen was continuously observed out in the magnetosheath during an interval of about 4 hours. The oxygen particles distribution function appeared to depend strongly on the orientation of the magnetosheath magnetic field, which varied during the period of observations. In particular, it was beam-like during southward magnetic field, with a very high velocity tangent to the magnetopause and perpendicular to the magnetic field; during predominantly northward magnetic field the distribution function was scattered both in energy and in angle, correspondingly the velocity was very low. Although the analysis of the data does not preclude that reconnection may be occurring at the magnetopause for this event, the observations have been very successfully reproduced by a model assuming that the oxygen particles cross the magnetopause simply because of their large gyroradius and taking into account the combined effect of the density gradient across the magnetopause and the magnetosheath convection. During southward magnetic field, the oxygen particles exit in the magnetosheath and, gyrating around the field, move tailward in the same direction as the magnetosheath convection, attaining a high tailward velocity, tangent to the magnetopause and perpendicular to the magnetic field. On the contrary, during northward magnetic field, the particles going out into the magnetosheath move sunward while being convected tailward so that the observed velocity is very low and they appear as an isotropic population attached to the magnetopause. *Sibeck et al.* [1987] elaborated on the motion of energetic ions oscillating between the magnetosphere and the magnetosheath at the subsolar magnetopause. Considering the motion of a single particle crossing the magnetopause, they pointed out that in a dawnward (duskward) field particles should move southward (northward); they did not take into account the magnetosheath convection as is appropriate at the subsolar magnetopause. In the present study we successfully reproduce the distribution functions and the oxygen velocity observed on the dusk flank of the magnetopause continuously, during over 3 hours, for any orientation of the magnetosheath field. The ion distribution functions have been inferred assuming that outside the magnetopause particles move back and forth along the magnetosheath magnetic field, have velocity component along the magnetopause directed as $\mathbf{n} \times \mathbf{b}$, and are shifted according to the magnetosheath convection. The moments of the model distribution functions have been computed in the same energy range (10–40 keV) as the observed ones.

[15] Although the overall trend of the observations is very well reproduced by our model, some quasi-periodic velocity enhancements, with period of about 5 min, superposed on the high velocity period of 0210–0320 UT, are not predicted. We interpret these velocity peaks as due to magnetopause surface motions. If the distance between the s/c and the magnetopause becomes larger, low-energy particles, with small gyroradii, will no longer be detected and at the same time the observed particle directions will be more tangent to the magnetopause. Therefore the particle distribution function will be reduced to high energy in a limited angular sector so that correspondingly, the bulk velocity will become larger. According to this interpretation, the almost periodic flow enhancements would correspond to oscillations of the magnetopause which vary the distance between the s/c and the particle source. *Mann et al.* [2002], by means of a detailed analysis of ground-based data (magnetometer, optical, and radar) from both the dusk and dawn sector ascertained the occurrence of global scale PC 5 ULF waves during the period of fast solar wind speed between 9 and 10 December 2000. In particular, Pc 5 wave activity is evident in CANOPUS magnetometer data between 2200 UT on 9 December and 0400 UT on 10 December 2000, while CANOPUS stations were in the dusk sector. The discrete frequency features of these ULF waves are consistent with the occurrence of magnetospheric waveguide modes and subsequently Field Line Resonances. In the same paper Cluster FGM observations were presented for the time interval 2200–2400 UT on 9 December 2000, showing quasi-periodic motion of the magnetosheath boundary layer of the same period (6–7 min) as the ULF pulsations observed on ground, which the authors considered to be the result of Kelvin-Helmoltz Instability (KHI) acting at the magnetopause. *Mann et al.* [2002]

concluded that Cluster and ground based coordinated observations strongly supports the hypothesis that magnetopause KHI induces the excitation of global scale wave guide modes. We believe that CIS plasma observations confirm the occurrence of the magnetopause surface oscillations also during the last part of the interval.

[16] **Acknowledgments.** We are grateful to the many engineers and scientists from CESR, IFSI, IRF, MPAe, MPE, UCB, UNH, and UW who made the development of the CIS instrument possible. The IFSI participation to the development of the CIS instrument and to this work was supported by the Agenzia Spaziale Italiana.

[17] Arthur Richmond thanks Nikolaos Paschalidis and another reviewer for their assistance in evaluating this paper.

References

Balogh, A., et al. (2001), The Cluster magnetic field investigation: Overview of in-flight performance and initial results, *Ann. Geophys.*, *19*, 1207–1217.

Crooker, N. U. (1979), Dayside merging and cusp geometry, *J. Geophys. Res.*, *84*, 951–959.

Daly, P. W., M. A. Saunders, R. P. Rijnbeek, N. Sckopke, and C. T. Russell (1984), The distribution of reconnection geometry in flux transfer events using energetic ion, plasma and magnetic data, *J. Geophys. Res.*, *89*, 3843–3854.

Eastmann, T. E., and L. A. Frank (1982), Observations of high-speed plasma flow near the earth's magnetopause: Evidence for reconnection?, *J. Geophys. Res.*, *87*, 2187–2201.

Fairfield, D. H. (1971), Average and unusual locations of the Earth's magnetopause and bow-shock, *J. Geophys. Res.*, *76*, 6700.

Gonzales, W. D., and F. S. Mozer (1974), A quantitative model for the potential resulting from reconnection with an arbitrary interplanetary magnetic field, *J. Geophys. Res.*, *79*, 4186–4196.

Gosling, J. T., J. R. Asbridge, S. J. Bame, W. C. Feldman, G. Paschmann, N. Sckopke, and C. T. Russell (1982), Evidence of quasi-stationary reconnection at the dayside magnetopause, *J. Geophys. Res.*, *87*, 2147–2158.

Gosling, J. T., M. F. Thomsen, S. J. Bame, and R. C. Elphic (1990), Plasma flow reversals at the dayside magnetopause and the origin of asymmetric polar cap convection, *J. Geophys. Res.*, *95*, 8073–8084.

Hudson, P. D. (1970), Discontinuities in an anisotropic plasma and their identification in the solar wind, *Planet. Space Sci.*, *18*, 1611–1622.

Lockwood, M., et al. (2001), Coordinated Cluster and ground-based instrument observations of transient changes in the magnetopause boundary layer during an interval of predominantly northward IMF: Relation to reconnection pulses and FTE signatures, *Ann. Geophy.*, *19*, 1613–1640.

Luhmann, , R. J. Walker, C. T. Russell, N. U. Crooker, J. R. Spreiter, and S. S. Stahara (1984), Patterns of potential magnetic field merging sites on the dayside magnetopause, *J. Geophys. Res.*, *89*, 1739–1742.

Mann, I. R., et al. (2002), Coordinated ground-based and Cluster observations of large amplitude global magnetospheric oscillations during a fast solar wind speed interval, *Ann. Geophy.*, *20*, 405–426.

Papamastorakis, I., G. Paschmann, N. Sckopke, S. J. Bame, and J. Berchem (1984), The magnetopause as a tangential discontinuity for large field rotation angles, *J. Geophys. Res.*, *89*, 127–135.

Paschalidis, N. P., E. T. Sarris, S. M. Krimigis, R. W. McEntire, M. D. Levine, I. A. Daglis, and G. C. Anagnostopoulos (1994), Energetic ions distributions on both sides of the Earth's magnetopause, *J. Geophys. Res.*, *99*, 8687–8703.

Paschmann, G., B. U. Ö. Sonnerup, I. Papamastorakis, N. Sckopke, G. Haerendel, S. J. Bame, J. R. Asbridge, J. T. Gosling, C. T. Russell, and R. C. Elphic (1979), Plasma acceleration at the Earth's magnetopause: Evidence for reconnection, *Nature*, *282*, 243.

Paschmann, G., G. Haerendel, I. Papamastorakis, N. Sckopke, S. J. Bame, J. T. Gosling, and C. T. Russell (1982), Plasma and magnetic field characteristics of magnetic flux transfer events, *J. Geophys. Res.*, *87*, 2159–2168.

Paschmann, G., I. Papamastorakis, W. Baumjohann, N. Sckopke, C. W. Carlson, B. U. Ö. Sonnerup, and H. Lühr (1986), The magnetopause for large magnetic shear: AMPTE/IRM observations, *J. Geophys. Res.*, *91*, 11,099–11,115.

Rème, H., et al. (2001), First multispacecraft ion measurements in and near the earth's magnetosphere with the identical Cluster Ion Spectrometry (CIS) experiment, *Ann. Geophys.*, *19*, 1303–1354.

Scholer, M. (1983), Energetic particle signatures near magnetospheric boundaries, *J. Geophys.*, *52*, 176–189.

Sibeck, D. G., R. W. McEntire, A. T. Y. Lui, R. E. Lopez, S. M. Krimigis, R. B. Decker, L. J. Zanetti, and T. A. Potmera (1987), Energetic magnetospheric ions at the dayside magnetopause: Leakage or merging?, *J. Geophys. Res.*, *92*, 12,097–12,114.

Sonnerup, B. U. Ö. (1974), The reconnecting magnetosphere, in *Magnetospheric Physics*, edited by B. M. McCormac, p. 23, D. Reidel, Norwell, Mass.

Sonnerup, B. U. Ö., G. Paschmann, I. Papamastorakis, N. Sckopke, G. Haerendel, S. J. Bame, J. R. Asbridge, J. T. Gosling, and C. T. Russell (1981), Evidence for magnetic reconnection at the Earth's magnetopause, *J. Geophys. Res.*, *86*, 10,049.

Speiser, T. G., D. J. Williams, and H. A. Garcia (1981), Magnetospherically trapped ions as a source of magnetosheath energetic ions, *J. Geophys. Res.*, *86*, 723–732.

Zong, Q.-C., B. Wilken, S. Y. Fu, T. A. Fritz, A. Korth, N. Hasebe, D. J. Williams, and Z.-Y. Pu (2001), Ring current oxygen ions escaping into the magnetosheath, *J. Geophys. Res.*, *106*, 25,541.

E. Amata, M. B. Bavassano Cattaneo, R. Bruno, V. Formisano, M. F. Marcucci, and G. Pallocchia, Istituto di Fisica dello Spazio Interplanetario, Consiglio Nazionale delle Ricerche, Via Fosso del Cavaliere 100, 00133 Roma, Italy. (amata@ifsi.rm.cnr.it; bice@ifsi.rm.cnr.it; bruno@ifsi.rm.cnr.it; formisan@ifsi.rm.cnr.it; federica@ifsi.rm.cnr.it; palloc@codif.ifsi.rm.cnr.it)

A. Balogh, Space and Atmospheric Physics Group, Blackett Laboratory, Imperial College, Prince Consort Road, London SW7 2BZ, UK.(a.balgoh@ic.ac.uk)

J. M. Bosqued, I. Dandouras, H. Rème, and J.-A. Sauvaud, CESR/CNRS, 9 Avenue du Colonel Roche, BP 4346, F-31028 Toulouse Cedex 4, France. (bosqued@cesr.fr; dandouras@cesr.fr; henri.reme@cesr.fr; sauvaud@cesr.fr)

C. W. Carlson and G. K. Parks, Space Science Laboratory, University of California, Berkeley, CA 94720, USA. (cwc@ssl.berkeley.edu; parks@ssl.berkeley.edu)

A. M. Di Lellis, AMDL s.r.l., Via Giovanni Angelini 33, 00149 Roma, Italy. (amdl@rm.iasf.cnr.it)

L. M. Kistler and E. Moebius, Space Science Center, University of New Hampshire, Durham, NH 03824, USA. (lynn.kistler@unh.edu; eberhard.moebius@unh.edu)

B. Klecker, Max-Planck-Institüt für Extraterrestrische Physik, Giessenbachstrassse, D-85748 Garching, Germany. (berndt.klecker@mpe.mpg.de)

A. Korth, Max-Planck-Institüt für Aeronomie, Max-Planck-Str. 2, 37191 Katlenburg-Lindau, Germany. (korth@linmpi.mpg.de)

R. Lundin, Swedish Institute of Space Physics, P. O. Box 812, S-98128 Kiruna, Sweden. (rickard@irf.se)

M. McCarthy, Geophysics Department, University of Washington, Box 351650, ATG Building, Seattle, WA 98195-1650, USA. (mccarthy@geophys.washington.edu)